Effect of pressure on Fe-Mg, Ni and Mn diffusion in (FeMg)SiO olivine

C. Holzapfel, S. Chakraborty, D.C. Rubie, D.J. Frost

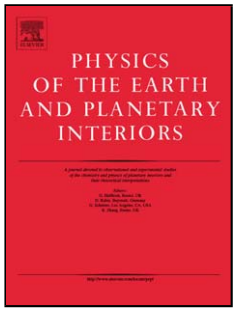

Title: Effect of pressure on Fe-Mg, Ni and Mn diffusion in $(Fe_xMg_{1-x})_2SiO_4$ olivine

Authors: C. Holzapfel, S. Chakraborty, D.C. Rubie, D.J. Frost

PII: S0031-9201(07)00082-9
DOI: doi:10.1016/j.pepi.2007.04.009
Reference: PEPI 4818

To appear in: *Physics of the Earth and Planetary Interiors*

Received date: 24-11-2006
Revised date: 10-4-2007
Accepted date: 11-4-2007

Please cite this article as: Holzapfel, C., Chakraborty, S., Rubie, D.C., Frost, D.J., Effect of pressure on Fe-Mg, Ni and Mn diffusion in $(Fe_xMg_{1-x})_2SiO_4$ olivine, *Physics of the Earth and Planetary Interiors* (2007), doi:10.1016/j.pepi.2007.04.009

Effect of pressure on Fe-Mg, Ni and Mn diffusion in $(Fe_xMg_{1-x})_2SiO_4$ olivine

C. Holzapfel[1*], S. Chakraborty[2], D.C. Rubie[1], D.J. Frost[1]**

[1]Bayerisches Geoinstitut, Universität Bayreuth, D-95440 Bayreuth, Germany

[2]Institut für Geologie, Mineralogie und Geophysik, Ruhr Universität Bochum, D-44780 Bochum, Germany.

[*]Now at:

Schleifring und Apparatebau GmbH,
Am Hardtanger 10,
D-82256 Fürstenfeldbruck,
Germany,

email: cholzapfel@schleifring.de

** Corresponding Author

email: Sumit.Chakraborty@rub.de

Abstract

The pressure dependence of Fe-Mg interdiffusion coefficients, as well as of diffusion coefficients of the trace elements Ni and Mn in olivine, have been determined from diffusion anneals carried out using oriented single crystals in multianvil presses. This is the first determination of activation volumes of diffusion of trace elements (Ni, Mn) in olivine. Results from an isothermal polybaric (1673 K, 6 - 12 GPa) and an isobaric polythermal (1623 - 1823 K, 12 GPa) set of experiments were combined to constrain

an internally consistent set of Arrhenius parameters for the diffusion processes. It is found that within the uncertainty of the data, (a) diffusion rates of Fe-Mg, Mn and Ni are very similar to each other at all conditions, consistent with more detailed observations from 1 atmosphere experiments (Petry et al., 2004), (b) apparent activation volumes using different fitting protocolls lie between 4 - 7 cm^3/mol, but a value of 5.3 ± 1.0 cm^3/mol (cf. Misener, 1974; Farber et al., 2000), describes the pressure dependence of diffusivity of these elements in olivine over its entire stability range (in pressure) adequately along the Ni-NiO fO_2 buffer, (c) the activation volume at constant fO_2 is higher, ~ 7 cm^3/mol and (d) at depths corresponding to the lowermost stability of olivine (~12 GPa), activation energies of diffusion are ~ 100 kJ/mol higher than at near surface conditions, which means that closure temperatures are higher by several hundred degrees.

Along geothermal gradients within the Earth, diffusion rates increase with depth in the lithosphere but decrease with depth, in spite of the increase in temperature, in the convective asthenospheric part of the mantle. Consequently, there is a maxima in diffusion rates at the lithosphere - asthenosphere boundary and for the olivine part of the mantle, this is likely to be the region where most geochemical mixing and eradication of heterogeneities occur.

Keywords

diffusion, olivine, multianvil apparatus, activation volume

1. Introduction

The kinetics of a variety of mantle processes, such as the chemical equilibration of

melt inclusions in olivine (e.g. Cottrell et al., 2002; Gaetani and Watson, 2002) and transformations between olivine and wadsleyite at the 410 km seismic discontinuity (Rubie, 1993a; Solomatov and Stevenson, 1994), depend on the rates of diffusion of elements such as Fe-Mg, Ni and Mn. Most diffusion coefficients for upper-mantle minerals have been determined at atmospheric pressure, where the effects of temperature, composition and oxygen fugacity have been well explored. Although the effect of pressure on diffusion is expected to be small, ignoring the effect for processes occurring at pressures of the Earth's upper mantle can cause errors of up to two orders of magnitude in estimates of diffusion rates and time scales. Experimental difficulties have hindered the precise determination of diffusion coefficients at high pressures. Following early studies (Misener, 1974; Elphick et al., 1985), a number of determinations at high pressure have now been carried out, as reviewed by Béjina et al. (2003) and summarized below. Nonetheless, problems still remain in characterizing the pressure dependencies of diffusion rates in key mantle minerals, as well as in the interpretation of high-pressure diffusion data in general.

To address these issues, we have determined diffusion coefficients for Fe-Mg, Ni and Mn in olivine over a range of pressures at constant temperature (1673 K, 6 - 12 GPa) as well as over a range of temperatures at constant pressure (1623 - 1823 K, 12 GPa). These data enable us to clarify the relationship between activation volume of diffusion at constant oxygen fugacity and apparent activation volumes typically determined along an oxygen fugacity buffer. The results, considered in conjunction with typical geothermal gradients, reveal that the lithosphere – asthenosphere boundary of the mantle is a zone of maximum mixing efficiency.

2. Previous Studies

Numerous studies have been performed of the rates of diffusion of divalent cations in

olivine at 1 bar, elevated temperatures and varying oxygen fugacities (Clark and Long, 1971; Buening and Buseck, 1973; Misener, 1974; Nakamura and Schmalzried, 1984; Hermeling and Schmalzried, 1984; Jurewicz and Watson, 1988; Morioka and Nagasawa, 1991; Chakraborty, 1997; Ito et al., 1999; Petry et al., 2004; Coogan et al., 2005). Differences that exist between the different datasets have been discussed by Chakraborty (1997) and Petry et al. (2004). High-pressure Fe-Mg interdiffusion experiments, performed up to 3.5 GPa by Misener (1974) and Farber et al. (2000), gave activation volumes of 5.5 and 5.4 $cm^3\ mol^{-1}$, respectively. Jaoul et al. (1995) determined Fe-Mg diffusion rates at relatively low temperatures (873-1173 K) at 3-9 GPa and concluded that the activation volume is essentially zero. Chakraborty et al. (1994) investigated Mg tracer diffusion in Mg_2SiO_4 forsterite as a function of pressure and determined an activation volume of 1-3.5 $cm^3\ mol^{-1}$. However, because the point defect chemistry of pure forsterite is different from that of Fe-bearing olivine, differences in diffusion behavior are to be expected. Finally, Chakraborty et al. (1999) investigated Fe-Mg interdiffusion at pressures between 9 and 15 GPa in olivine and wadsleyite and compared diffusion rates in the two polymorphs under similar conditions. In addition to uncertainties in oxygen fugacity, the limited data set of their study did not enable activation volumes to be determined. Recent discussions of oxygen fugacity dependence of diffusion coefficients in olivine, and problems with the experimental determination of this quantity, may be found in Petry et al. (2004) and Coogan et al. (2005).

In order to address the issue of oxygen fugacity in this study, we have investigated diffusion in olivine at high pressure using two kinds of capsule materials - Au, as used by Chakraborty et al. (1999) and Ni in contact with a layer of NiO as used in Holzapfel et al. (2003, 2005). The new results enable oxygen fugacity to be

estimated in experiments employing Au capsules and allow the activation volume for diffusion in olivine to be estimated using data obtained over the pressure range from 1 bar to 12 GPa.

3. Experimental procedure

3.1. *Starting materials*

All experiments were performed on diffusion couples prepared from the same two single crystals. One end member was a synthetic Mg_2SiO_4 forsterite single crystal, grown using the Czochralski method by H. Takei at Tohoku University. It is the same crystal (Fo1) as used by Chakraborty et al. (1994), where trace element contents are also reported. The Fe content of this crystal varies between 120 and 180 ppm. The Fe-bearing sample was a natural single crystal from San Carlos with an average value of Mg/(Mg+Fe) = 0.94, containing 3000 ppm Ni and 1500 ppm Mn. Both crystals were oriented along the crystallographic c-direction by Laue backscatter diffraction such that the [001] axis was perpendicular to the diffusion interface. After the diffusion experiments, the orientations of both crystals were checked by electron backscatter diffraction (EBSD). The c-axes were always found to lie in the diffusion plane perpendicular to the diffusion interface within an error of < 4°.

For preparation of diffusion couples, the crystals were cut into thin polished slices ~250 μm thick, from which discs were drilled out with a diameter of 250 μm (Au-capsule experiments) or 950 μm (Ni-NiO capsules). The olivine slices were polished using diamond spray (Struers) down to 0.25 microns. The two single-crystal components of the diffusion couple were inserted into the capsule with the two polished faces in contact with each other.

3.2. *Capsule Materials*

In previous studies of diffusion at high pressure, several different capsule materials have been employed (Béjina et al., 2003). The ideal capsule material does not interact chemically with the sample (e.g., no Fe loss), buffers the oxygen fugacity and is mechanically weak in order to minimize differential stresses imposed on the diffusion couple. It is difficult to meet all these requirements simultaneously with any single capsule material. Therefore, two different capsule materials were used in this study. In most experiments, mechanically-weak Au capsules were employed (Chakraborty et al., 1999). In order to constrain oxygen fugacity close to the Ni-NiO buffer, some experiments were also performed using Ni capsules with added NiO powder (similar to Holzapfel et al., 2003, 2005).

The gold capsules were prepared by drilling a 250 μm diameter hole in gold wire of 1 mm diameter. Discs of the single crystals of olivine were carefully inserted and the container was closed by deforming the end of the wire (Chakraborty et al., 1999). The Ni capsules were prepared from rolled Ni foil. After inserting the two olivine single crystals, NiO powder (previously dried at 1273 K) was placed on top of the diffusion couple. The capsule was then closed by folding over the end of the Ni foil. As noted by Farber et al. (2000), Ni from the buffer assemblage entering the olivine single crystals at the ends removed from the diffusion zone also defines the ambient silica activity of the experiment through the equilibrium $2NiO + SiO_2 = Ni_2SiO_4$.

3.3. *High-Pressure diffusion experiments*

Diffusion experiments were performed between 8 and 12 GPa using a 500 t Walker-style multianvil apparatus. The pressure assembly consisted of a "14/8" configuration consisting of an MgO octahedron with an edge length of 14 mm and WC cubes with a

truncation edge length of 8 mm (Fig. 1). High temperature was produced using a $LaCrO_3$ resistance furnace with a stepped wall thickness in order to reduce temperature gradients to <20 K mm^{-1} (Rubie et al., 1993b). The $W_{97}Re_3$-$W_{75}Re_{25}$ thermocouple junction was located within the middle section of the furnace, as close as possible to the sample. No pressure correction for the EMF of the thermocouple was applied.

Pressure was calibrated using the quartz-coesite and Mg_2SiO_4 olivine-wadsleyite transformations (Keppler and Frost, 2005). After heating (at approximately 2 K/sec), temperature was controlled to within ±1 K. Samples were quenched by switching off the power to the furnace, which resulted in the temperature dropping to below 573 K in less than 2 sec. The pressure and temperature conditions of the diffusion experiments, together with the capsule types used, are listed in Table 1. Temperatures of experiments in which Au capsules were used were limited at lower pressures by the melting point of Au (~1673 K at 6 GPa; Young, 1991). One set of experiments was performed at a constant temperature of 1673 K in order to study the effect of pressure on diffusion. In a second set of experiments, temperature was varied between 1623 K and 1823 K at a fixed pressure of 12 GPa to determine the effect of temperature. Most experiments were run for 24 hours, with the exception of an experiment at 1623 K and 12 GPa, which lasted for 72 hours. At these conditions the lengths of the resulting diffusion profiles were 8-20 µm.

4. Profile analysis and diffusion coefficient determination

After the experiments, the sample assemblies were mounted in epoxy resin and prepared to expose a polished section through the middle of the diffusion couple. Concentration profiles were measured by electron microprobe analysis (EPMA) using

a Cameca SX-50 equipped with 4 wavelength dispersive spectrometers and a Jeol JXA 8900 RL equipped with 5 wavelength dispersive spectrometers. Special attention was paid to optimizing the lateral spatial resolution of the microprobe beam by aligning the objective aperture with the help of a cathodoluminenscence spot on SnO_2 and by correcting for astigmatism at high magnifications. San Carlos olivine was used as a standard for all major elements while NiO and rhodonite were used for Ni and Mn, respectively. Acceleration voltages of 15 or 20 kV and probe currents between 15 and 20 nA were used. For major elements counting times between 5 and 20 sec were adequate (Reed, 1996) but for the trace elements, Ni and Mn, counting times of 120-150 sec were required. The relative statistical error of the measurements is less than 2% at these conditions (Petry, 2004).

Diffusion profiles were symmetric within the compositional range investigated. Hence a solution of the diffusion equation for a composition-independent diffusion coefficient could be employed (Crank, 1979):

$$\frac{C(x,t)-C_r}{C_l-C_r}=\frac{1}{2}erfc\left(\frac{x}{2\sqrt{Dt}}\right) \qquad (1)$$

where C_l and C_r denote the initial compositions of the two crystals of the diffusion couple, $C(x,t)$ is the composition at position x along the profile and time t, and D is the diffusion coefficient. Equation 1 is valid for the initial conditions:

$C = C_l, x < 0, t = 0$

$C = C_r, x > 0, t = 0 \qquad (2)$

and the boundary condition of two semi-infinite media (i.e., the diffusion profile does not reach the ends of the diffusion couple).

5. Results and Discussion

5.1. *Characterization of diffusion couples after the experiments*

All samples were examined optically, by high resolution backscattered electron imaging (Figure 2) and elemental mapping before measurement of diffusion profiles. IR spectroscopy was used to characterize OH contents of the samples. Diffusion fronts were found to be regular and parallel to the crystal interface with one exception. In experiment 20CS6, the central part of the diffusion couple sheared between two cracks (probably during initial compression) and recrystallized. Therefore, in this sample, diffusion profiles were measured in undisturbed areas outside the shear zone where the original single crystal structure remained intact. In some of the experiments, the two crystals of the diffusion couple separated at the interface during decompression and/or sample preparation. The separation distance was much less than 1 μm and therefore has an insignificant effect on the analysis of the shape and length of the diffusion profiles.

Water, dissolved in the crystal structure as OH, potentially influences rates of cation diffusion in olivine (Mei and Kohlstedt, 2000; Chakraborty and Costa, 2004; Kubo et al., 2004, Hier-Majumder et al., 2005). To characterize the water contents of our samples after the diffusion experiments, polarized infrared spectra were measured on sample 8CS10.5 employing a Bruker IFS 120 HR high resolution FTIR spectrometer. The forsterite contained no detectable water whereas the Fe-bearing San Carlos olivine contained ~25 ppm by weight based on the absorption correction of Paterson (1982). This is below the concentration range where water becomes effective in enhancing diffusion rates of Fe-Mg in olivine (Hier-Majumder et al., 2005).

5.2. Concentration profiles and diffusion coefficients

Typical compositional profiles for Fe, Mg, Ni, and Mn are shown in Fig. 3. The profiles are symmetric for all the experiments described here, in contrast to the observation of strongly asymmetric profiles by Chakraborty (1997). This difference can be explained by the limited compositional range of this study (Fo_{100}-Fo_{94}). The diffusion coefficients presented here are therefore representative for the average composition of the diffusion couple (Mg# = 0.97).

Diffusion coefficients were determined by fitting Equation 1 to the concentration profiles using a nonlinear least squares fitting routine (Mathematica Software, Version 4.2.0.0) and are listed in Table 1. Errors were estimated by considering different profile measurements on the same sample, as well as differences in diffusion coefficients retrieved from different samples annealed at the same conditions. The error is ~0.2 log units for Fe-Mg interdiffusion, whereas for Ni and Mn diffusion coefficients, errors of 0.3 and 0.4 log units, respectively, were estimated. The larger errors for Ni and Mn are caused by the relatively large analytical scatter for these two trace elements (Fig. 3). Including uncertainties in pressure and temperature, the overall errors for the high pressure diffusion coefficients are likely to be ~0.3 log units for Fe-Mg interdiffusion, ~0.4 log units for Ni and ~0.5 log units for Mn diffusion (Holzapfel, et al., 2003).

Because some profiles are only 8-10 µm long, convolution effects in the microprobe analysis may influence the determined diffusion coefficients. The possible effect of profile broadening, due to the finite excitation volume of the X-rays, was estimated using the algorithm developed by Ganguly et al. (1988). The standard deviation of the X-ray excitation volume, assuming a Gaussian intensity distribution, was determined to be better than 0.46 µm by analyzing across a sharp Al_2O_3-MgO

boundary in a multianvil sample assembly. Considering the experimental uncertainties (see above), profiles as short as 8 μm would still yield reliable diffusion coefficients (within 12% of the true value; see Eq. 20 in Ganguly et al., 1988). In order to verify this conclusion, two samples, 6CS10 and 17CS12 (Table 1), with diffusion profile lengths of 10 and 8 μm, respectively, were analyzed by EDX-STEM (energy dispersive spectrometry employing scanning transmission electron microscopy) following the procedure of Meißner et al. (1998). In both cases (the example of sample 17CS12 is shown in Fig. 4), the difference between the diffusion coefficients determined by fitting Equation 1 to the STEM profile and the EPMA profile is on the order of 30% at most, which is larger than that estimated using the algorithm of Ganguly et al. (1988). As outlined above, diffusion coefficients determined on the same sample using different profiles differ by up to 0.2 log units (relative error ~50%). The error due to convolution is considerably less than this value for the profile lengths obtained in this study and therefore no explicit corrections have been made.

The profiles of Fig. 4 suggest that the asymmetry resulting from the composition-dependence of diffusion coefficients can be resolved by EDX-STEM but not by EPMA. For both samples, an asymmetric fit using the composition dependence factor, $\exp(6.9X_{Fe2SiO4})$, determined at 1 bar (Chakraborty, 1997; Dohmen et al., 2007a), is compatible with the TEM profiles but not with the EPMA profiles (Fig. 4). Thus, based on the compositional dependence of Charkraborty (1997), to calculate Fe-Mg interdiffusion coefficients at $X_{Fe2SiO4} = 0.90$, the average olivine composition in the upper mantle, it is necessary to add 0.2-0.3 log units to the data obtained in this study for $X_{Fe2SiO4} = 0.97$. Note that the existence of slight asymmetry may explain the mismatch (see above) in estimates of the effect of convolution using the formulation

of Ganguly et al. (1998) and STEM-EDX profile analysis, respectively, because the former was developed for symmetric profiles.

5.3. *Pressure dependence at 1673 K*

Diffusion coefficients obtained at 1673 K and pressures of 6-12 GPa (Table 1) are plotted together with 1-bar values (Chakraborty, 1997; Petry et al., 2004) as a function of pressure in Fig. 5. In all subsequent figures, the results obtained using Au capsules at one pressure and temperature are grouped into one data point for clarity. The calculations presented later use the individual values. The 1-bar value plotted in Fig. 5a, $\log D_{Fe-Mg}^{Fo_{97}}$ = -14.42, was obtained by using the Arrhenius relationship and compositional dependence reported by Chakraborty (1997). An oxygen fugacity exponent of 1/5 was used, based on Nakamura and Schmalzreid (1983) as well as recent experimental results (Petry et al., 2004; Dohmen et al., 2007a). For Ni, the 1-bar diffusion coefficient was obtained from Petry (1999) and Petry et al. (2004) and corrected for composition and fO_2 using dependencies given by Petry et al. (2004). This yields log D_{Ni} = -13.96 at 1673 K. For Mn, data on composition and fO_2 are unavailable and only the high pressure data were fitted in order to determine the activation volume.

Within the experimental uncertainties, diffusion coefficients determined using Ni-NiO capsules are similar to those obtained using Au capsules (Fig. 5A). This implies that fO_2 in the Au-capsule experiments is close to the Ni-NiO buffer. However, there may be systematic differences that cannot be resolved using the current data set. Therefore, in order to determine if there is a statistically significant difference, we have calculated activation volumes by fitting (1) the complete data set and (2) results obtained in different capsule types separately.

Diffusivities determined at 11 GPa are anomalously high compared with data obtained at other pressures, especially for Fe-Mg interdiffusion (Fig. 5). This phenomenon was also observed by Chakraborty et al. (1999). The cause for this apparent "spike" is uncertain, but it is based on more than one experiment and thus cannot be regarded as a single outlier. Given the absence of any plausible explanations for the results at 11 GPa, we have chosen to exclude them from the data set when performing fits to determine activation volumes. Thus, all further discussion refers to an apparent activation volume obtained from a linear Arrhenian fit to all other diffusion data and allows the pressure dependence of diffusion coefficients in olivine to be calculated within experimental error using an Arrhenius type equation. The validity of this approach is tested experimentally in the next section.

Table 2 lists the activation volumes obtained from linear fits to the diffusion coefficients shown in Fig. 5, for Fe-Mg interdiffusion, Ni diffusion and Mn diffusion. In each case we explored the effects of alternative fits by using (a) data from Ni-NiO capsules only, (b) data from Au capsules only, and (c) the entire dataset; in addition, we repeated each fitting exercise with and without the 1 bar values. Depending on which data subset is used, the activation volume for Fe-Mg interdiffusion lies in the range 3.8 - 6.3 cm^3 mol^{-1}. Considering the errors, the differences between the activation volumes derived for different data sets are not statistically significant (Fig. 5A, Table 2). The combined analysis further suggests that the values derived from Au capsule experiments are representative of diffusivities at an oxygen fugacity close to or slightly above the Ni-NiO buffer. This observation is also justified considering the fact that extrapolating the Au data to one bar (8 GPa of extrapolation) leads to a log (D) value of -14.9, which is just 0.6 log units below the 1 bar data point at Ni-NiO (see above).

For Ni diffusion, activation volumes in the range 5.4-7.0 cm^3 mol^{-1} are obtained for the same exercise. Within the relatively large uncertainty, we concluded that the activation volumes for Ni diffusion and Fe-Mg diffusion are similar (Table 2). In the case of Mn, the large scatter in the data and the absence of an estimate of the diffusivity at 1 bar result in a large uncertainty in the activation volume. Only the fit using all the data (Fig. 5c) results in a statistically significant activation volume of 4.6 ± 1.7 cm^3 mol^{-1}, which is similar to the values derived for Fe-Mg interdiffusion and Ni diffusion (Table 2). Using the fit to all Mn data, an extrapolation to 1 bar results in a value of log (D_{Mn}) = -14.9, which, within uncertainties (see above), is close to the value for Fe-Mg interdiffusion (Fig. 5c).

Based on the results presented here, it can be concluded that diffusion coefficients for divalent cations in olivine are similar to each other, as observed in studies at 1 bar (e.g. Petry et al., 2004). The activation volumes for these diffusing species (Fe-Mg, Ni and Mn) are also similar and lie in the range 4 to 7 cm^3 mol^{-1}. Because there is no statistically significant difference between diffusion coefficients determined from experiments using Au capsules and Ni-NiO capsules, the activation volume derived by fitting all data for a particular cation likely provides the best estimate of the activation volume at 1673 K and at an fO_2 close to the Ni-NiO buffer. For Fe-Mg interdiffusion, this value is 5.3 ± 0.6 cm^3 mol^{-1}. We recommend this value for calculation of pressure dependence of the other elements as well, although consideration of formal errors suggests a range of 4 - 7 cm^3 mol^{-1}. This best fit value is also essentially the same as that found by Misener (1974) and Farber et al. (2000) and is tested with independent experimental data in the next section.

The activation volumes have been derived from diffusion coefficients that were

determined at an fO_2 corresponding to the Ni-NiO buffer. Strictly speaking, however, activation volumes should be defined at a constant oxygen fugacity and not at oxygen fugacities that are varying with P and T along an oxygen fugacity buffering reaction. We find that the variation of fO_2 at 1673 K is from -5.8 log units at 1 bar to -2.5 log units at 12 GPa, assuming that the volume change of the Ni-NiO buffering reaction is constant as a function of pressure. This change in fO_2 corresponds to a change of 0.7 log units in the diffusivity (using values from Ride, 1991, as discussed below). Correcting the data by this factor, an activation volume of 5.3 cm^3 mol^{-1} along the Ni-NiO buffer corresponds to a value of 7.1 cm^3 mol^{-1} at a constant oxygen fugacity.

5.4. Temperature dependence at constant pressure (12 GPa)

To directly constrain the temperature dependence of diffusion coefficients at high pressure, experiments have been performed between 1623 K and 1823 K at 12 GPa using mainly Au but also Ni capsules. As shown in the previous section, results from experiments performed in Au and Ni capsules are very similar. Further, these measurements in conjunction with other available results constitute an independent determination of the activation volume of diffusion and provide a test of the values inferred above.

Diffusion coefficients are given in Table 1 and are displayed in Arrhenius plots in Fig. 6. In all cases, trends are linear, indicating that the diffusion mechanism for divalent cations does not change at 12 GPa over the temperature range 1623-1823 K. A linear Arrhenian fit to the data at 12 GPa yields an activation energy (E_a^*) of 346±59 kJ mol^{-1} for Fe-Mg interdiffusion, 329±36 kJ mol^{-1} for Ni diffusion , and 233±79 kJ mol^{-1} for Mn diffusion. The errors correspond to the 1-σ standard deviation of the linear

fits.

Figure 7 shows a superposition of results obtained for Fe-Mg interdiffusion, Ni diffusion and Mn diffusion and it can be seen that the values are almost identical within the uncertainties. This implies again that within the temperature interval investigated, diffusivities of divalent cations are very similar, as observed at 1 bar (Petry et al., 2004**)**. Therefore, analogous to the isothermal data series discussed earlier, we believe that the 100 kJ mol^{-1} lower activation energy obtained by simple statistical fitting of the noisy data for Mn is probably an artifact. These data indicate, therefore, that Fe-Mg interdiffusion coefficients and activation energies can be reliably used to describe diffusion rates of divalent cations other than Ca at high pressures.

Having obtained these activation energies at high pressures (12 GPa), we can now verify the consistency with other known Arrhenian parameters, namely, the activation energies determined at 1 bar (Petry et al., 2004), E_a^1 , and the activation volumes determined in the last section. These are related through

$$\left(\frac{\partial \ln D}{\partial \frac{1}{T}}\right)_P = -\frac{E_a^P}{R} = -\frac{E_a^1 + PV_a}{R} \qquad (3)$$

where E_a^P is the activation energy at high pressure and constant oxygen fugacity assuming that the preexponential factor is pressure independent. However, an additional complication arises because the activation energies at 1 bar were determined at constant fO_2 whereas the high-pressure data were collected along an

oxygen fugacity buffer (Ni-NiO). The two activation energies may be related by expressing the total differential of the logarithm of diffusion coefficient as a function of pressure, temperature and oxygen fugacity (e.g. see Ganguly et al. 1998). At constant pressure,

$$\left(d\ln D\right)_P = \left(\frac{\partial \ln D}{\partial \frac{1}{T}}\right)_{fO_2,P} \left(d\frac{1}{T}\right)_P + \left(\frac{\partial \ln D}{\partial \ln fO_2}\right)_{P,\frac{1}{T}} \left(d\ln fO_2\right)_P \qquad (4)$$

Equation 4 can be rewritten as:

$$\left(d\ln D\right)_P = -\frac{E_a^{P,c}}{R}\left(d\frac{1}{T}\right)_P + \left(\frac{\partial \ln D}{\partial \ln fO_2}\right)_{P,\frac{1}{T}} \left(\frac{d\ln fO_2}{\partial \frac{1}{T}}\right)_{NNO,P} \left(d\frac{1}{T}\right)_P \qquad (5)$$

where $E_a^{P,c}$ is the activation energy at high pressure and constant fO_2. Hence, the activation energy at high pressure including the effect of fO_2, $E_a^{*,P}$ is:

$$E_a^{*,P} = E_a^{P,c} - R\left(\frac{\partial \ln D}{\partial \ln fO_2}\right)_{P,\frac{1}{T}} \left(\frac{d\ln fO_2}{\partial \frac{1}{T}}\right)_{NNO,P} \qquad (6)$$

In order to evaluate the magnitude of this effect, we use the exponent 1/5 (as discussed above) for describing the effect of oxygen fugacity on the Fe-Mg interdiffusion coefficient. The temperature dependence of oxygen fugacity corresponding to the Ni-NiO buffer (NNO) at 12 GPa is much less well constrained. As in the previous section, if we make the reasonable assumption of a pressure independent volume change of the Ni oxidation reaction and use numerical values from Ride (1991) then the apparent activation energy at 12 GPa, $E_a^{*,12}$ along the NNO buffer can be described according to Equation 6 by

$$E_a^{*,12} = E_a^{12,c} + 72 \text{ kJ mol}^{-1} \quad (7)$$

Finally, combining Eqns. (3) and (7) one obtains

$$E_a^{1,c} + PV_a + 72 \text{ kJ mol}^{-1} = E_a^{*,12} \quad (8)$$

where V_a is the activation volume at constant oxygen fugacity.

In making this connection we have assumed, following the findings in the last section, that fO_2 in experiments in Au capsules is close to that imposed by a Ni-NiO buffer. Inserting numerical values, we find that the calculated value of $E_a^{*,12}$ from equation (8), 366 kJ mol^{-1}, differs from the directly determined value by 20 kJ mol^{-1}, which is an acceptable deviation considering the various sources of uncertainty (activation energy, activation volume and pressure dependence of oxygen fugacity). Thus, within the uncertainty of the data, the activation energies and volumes derived above constitute an internally consistent set of Arrhenian parameters.

5.5. Comparison with previous results

The results for Fe-Mg interdiffusion obtained in this study are shown in Figure 8 together with the results of other studies in which Fe-Mg interdiffusion was examined at high pressures and temperatures (Misener, 1974; Chakraborty et al, 1999; Farber et al 2000).

In Chakraborty et al. (1999), three experiments performed with Au capsules using a similar pressure cell assembly to that employed in this study were reported. The strong asymmetry in the profile shown for olivine in Fig. 2A of Chakraborty et al. (1999) indicates a considerable variation in diffusion coefficient along the diffusion

direction. Typically, such variation results from a compositional dependence of diffusivity. However, the dependence suggested by the asymmetry is much larger than that at 1 atmosphere and consequently the diffusion couple was carefully re-investigated using Electron Backscatter Diffraction (EBSD). This revealed that only the Fe-rich side of the crystal was oriented along [001] while the forsterite was oriented along [100]. The change in crystallographic orientation occurs sharply at the interface (within a distance of 1 μm). The known anisotropy of diffusion in olivine ($D_{[001]} \sim 6\ D_{[100]}$) explains the strong asymmetry observed in the profiles of Chakraborty et al. (1999) which is therefore not a result of an unusual compositional dependence of diffusivity, contrary to the statements in Chakraborty et al. (1999). The comparison of data for Fo_{86} at 9, 11 and 12 GPa for Fe-Mg interdiffusion given by Chakraborty et al. (1999) shows good agreement with results of the present study. Interestingly, this agreement extends to the value of the diffusion coefficient at 11 GPa (comparison not shown in figure), which is again much faster than that expected from a simple linear relationship between log D and pressure. The error bars were taken to be as large as in the present study because the experimental procedure was the same in both sets of experiments. The fO_2 of the experiments was estimated using the secondary calibration based on Ni capsules from this study, rather than using the calculations of Chakraborty et al. (1999).

Misener (1974) performed high pressure experiments up to 3.5 GPa in a piston cylinder apparatus. The Fe-Mg interdiffusion coefficient reported by Misener (1974) at 1373 K and $X_{Fe_2SiO_4} = 0.4$ was converted to a diffusion coefficient at 1673 K and $X_{Fe_2SiO_4} = 0.03$ using the activation energy and compositional dependence of Chakraborty (1997). Misener (1974) did not report any fO_2 for his experiments and so

no correction was made for the effect of fO_2. The datum is in very good agreement with the results from this study in terms of both the absolute value of diffusion coefficients as well as the pressure dependence. The activation volume of 5.5 cm^3 mol^{-1} obtained by Misener (1974) is, within errors, identical to the value derived in this study (5.3 ± 1.0 cm^3 mol^{-1}) along the Ni-NiO buffer.

Farber et al (2000) found very similar pressure dependence to that determined by Misener (1974) and this study. Their activation volume of 5.4 ± 4.0cm^3 mol^{-1}along the Ni-NiO buffer is in excellent agreement with the results presented in this study. However, the absolute values of the diffusion coefficients found by Farber et al (2000) are higher, by about an order of magnitude (0.8 log units), than those measured in this work. Inadequate resolution of the compositional dependence of diffusion coefficients and / or the use of polycrystalline samples as one end member of the diffusion couple in the study of Farber et al. (2000) are possible reasons for the discrepancy.

The experiments of Jaoul et al. (1995), carried out between 600 and 900^oC, employed San Carlos olivine covered with a thin layer of fayalite and the diffusion profiles were analyzed by Rutherford backscattering spectroscopy. The diffusion coefficients obtained in their study along the crystallographic [010] direction are faster than values obtained by down-temperature extrapolation of any data set other than that of Buening and Buseck (1973). Repeated recent measurements performed at 1 atmosphere using a number of different methods (Chakraborty 1997; Meißner et al. 1998; Petry et al 1999; Dohmen et al. 2007a; Düffels et al. 2004) indicate that the data of Buening and Buseck (1973) is too fast. Dohmen et al. 2007a demonstrate that this is most likely to

due to artefacts of measurement using older electron microprobes in the study of Buening and Buseck (1973). Internal inconsistencies in the data reduction procedure and arguments of Jaoul et al. (1995) make this work difficult to evaluate. For example, it is not clear for which olivine compositions the data were determined and the rationale for the use of their Eqn. 4 for data reduction is not very clear, to mention two aspects. In any case, we note that the differences between activation volumes determined by Misener (1974) and Jaoul et al. (1995) cannot be due to a change in diffusion mechanism from intrinsic to extrinsic, as claimed by Jaoul et al. (1995), because diffusion in the temperature range studied by Misener (1974) was not intrinsic. It has been shown that over the temperature range of the experiments of Misener (1974), the TaMED (Transition metal extrinsic) mechanism operates in Fe-bearing olivine (Chakraborty 1997, Dohmen et al., 2007b).

6. Summary of Conclusions and Implications

By measuring diffusion coefficients over the entire pressure range of the olivine stability field and determining the pressure dependence of these coefficients using alternate approaches, we have been able to constrain the apparent activation volume for Fe-Mg diffusion in olivine to be 5.3 cm^3 mol^{-1} along the Ni-NiO oxygen buffer, which is consistent with the results of Misener (1975) and Farber et al. (2000) but not with those of Jaoul et al. (1995). The activation volume for diffusion at constant absolute fO_2 is slightly higher, i.e. 7 cm^3 mol^{-1}, because the pressure dependence of the fO_2 buffer reaction becomes incorporated into the activation volume. Diffusion under hydrous conditions occurs by a different mechanism and the activation volume for that process has been shown to be much higher (~ 16 cm^3/mol, Hier-Majumder et al., 2005). Determined activation energies of diffusion in this study are up to 100 kJ/mol higher at depth in the upper mantle in comparison to 1 atmosphere (e.g. 346

kJ/mol at 12 GPa vs. 220 kJ/mol at 1 atmosphere). This results in an increase of closure temperatures by several hundred degrees. For example, a spherical olivine grain of radius 1 mm cooling at 1 K/myrs would have a closure temperature of ~ 675 °C at atmospheric pressure, but ~ 880 °C at a depth of 150 Km and 1175 °C at a depth of 400 Km (ignoring anisotropy of diffusion in olivine). These numbers would be slightly higher for faster cooling rates (e.g. ~ 750 °C, 980 °C and 1270 °C, respectively, for a cooling rate of 10 K/myrs.).

We have also measured, for the first time, the diffusion rates of trace elements such as Ni and Mn in olivine under high pressures. Analogous to the findings from atmospheric pressure experiments (Petry et al., 2004), diffusion rates of these elements are found to be very close to those of Fe-Mg. Activation volumes for diffusion of these elements along the NNO buffer are also similar, lying within the range of 4-7 $cm^3 mol^{-1}$, but with larger uncertainties than for the activation volume for Fe-Mg diffusion.

Figure 9 illustrates how diffusion rates of divalent cations (other than Ca) in olivine change with depth along a geotherm in the mantle. The parameters for the lithospheric geothermal gradient are from Turcotte and Schubert (1982) and for the adiabat in the asthenosphere from Katsura et al. (2004). Arrhenius parameters for temperature dependence of diffusion rates were taken from Chakraborty (1997) and it is assumed that the oxygen fugacity is maintained close to the Ni-NiO buffer. It is found that diffusion rates increase with depth in the lithospheric part of the mantle due to the steep thermal gradient. However, along a mantle adiabat in the asthenosphere between 150 and 400 km depth the diffusivities in olivine actually *decrease* by approximately

1 log unit even though the temperature increases from ~1650 K to 1730 K because the thermal gradient is much weaker. If the pressure effect is not taken into account, the diffusion coefficient would *increase* by a factor of 10 over the same depth interval. The diffusion coefficient at 400 km depth would be overestimated by ~ 2-3 orders of magnitude (Fig. 9). This reversal in diffusion rates in olivine, combined with the variation of closure temperatures with depth, has important consequences for kinetic and geodynamic processes that have not been explored in previous studies (e.g. Solomatov and Stevenson, 1994). The behavior observed in this study indicates that the lithosphere - asthenosphere boundary region is the place where heterogeneities in the olivine bearing mantle are most efficiently destroyed, rather than in the bulk of the convective asthenosphere part of the mantle. This effect is most likely further accentuated by the initiation of melting at this depth.

8. Acknowledgments

We thank Prof. Takei for generously donating us the forsterite crystal used in this study. We appreciate constructive reviews from T. Kubo and an anonymous reviewer that helped improve the manuscript. SC acknowledges support from the SFB 526 program of the DFG (German Science Foundation).

References

Béjina, F., Jaoul, O., and Liebermann, R. C., 2003. Diffusion in minerals at high pressure: A review. Phys. Earth Plan. Int., 139: 3-20.

Buening, D. K., and Buseck, P. R., 1973. Fe-Mg lattice diffusion in olivine. J.

Geophys. Res., 78: 6852-6862.

Chakraborty, S., 1997. Rates and mechanisms of Fe-Mg interdiffusion in olivine at 980-1300°C. J. Geophys. Res., 102: 12317-12331.

Chakraborty, S., Farver, J.R., Yund, R.A., and Rubie, D. C., 1994. Mg tracer diffusion in synthetic forsterite and San Carlos olivine as a function of P, T and fO_2. Phys. Chem. Minerals, 21: 489-500.

Chakraborty, S., Knoche, R., Schulze, H., Rubie, D. C., Dobson, D., Ross, N.L., and Angel, R.J., 1999. Enhancement of cation diffusion rates across the 410-kilometer discontinuity in Earth's mantle. Science, 283: 362-365.

Chakraborty, S. and Costa, F. (2004) Fast diffusion of Si and O in San Carlos olivine under hydrous conditions, Goldschmidt Conference, Copenhagen, Denmark

Clark, A. and Long, J, 1971. The anisotropic diffusion of nickel in olivine. In J. Sherwood, A. Chadwick, W. Muir and F. Swinton (Editors). Diffusion processes: 511-521.

Coogan, L., Hain, A., Stahl,.S. and Chakraborty, S. (2005) Experimental determination of the diffusion coefficient for calcium in olivine between 900°C and 1500°C. Geochim. Cosmochim. Act., 69, 14, 3683 - 3694.

Cottrell, E., Spiegelmann, M., and Langmuir, C. H., 2002. Consequences of diffusive

reequilibration for the interpretation of melt inclusions. Geochemistry Geophysics Geosystems, 3: U1-U26.

Crank, J., 1979. The Mathematics of Diffusion. Oxford University Press, Oxford

Dohmen, R., Becker, H.-W., and Chakraborty, S., 2007a. Fe-Mg diffusion coefficients in olivine. Part I: Experimental determination between 700 and 1200 °C as a function of composition, crystal orientation and oxygen fugacity. Phys. Chem. Min., in print.

Dohmen, R. and Chakraborty, S. 2007b. Fe-Mg diffusion in olivine II: point defect chemistry, change of diffusion mechanisms and a model for calculation of diffusion coefficients in natural olivine. Phys. Chem. Min., in print.

Dueffels, K., Chakraborty, S., and Brenker, F., 2004. Enhacement of diffusion rates in olivine during evaporation - an example of reactive diffusion in a mineralogical system. EMPG Meeting Proceedings, Frankfurt, Germany.

Elphick, S. C., Ganguly, J., and Loomis, T. P., 1985. Experimental determination of cation diffusivities in aluminosilicate garnets: I. Experimental methods and interdiffusion data. Contrib. Mineral., 90: 36-44.

Farber, D. L., Williams, Q., and Ryerson, F.J., 2000. Divalent cation diffusion in Mg_2SiO_4 spinel (ringwoodite), β phase (wadsleyite), and olivine: Implications for the electrical conductivity of the mantle. J. of Geophy. Res., 105: 513-529.

Gaetani, G. A., and Watson, E. B., 2002. Modelling the major-element evolution of olivine-hosted melt inclusions. Chem. Geol., 183: 25-41.

Ganguly, J., Bhattacharya, R. N., and Chakraborty, S., 1988. Convolution effect in the determination of compositional profiles and diffusion coefficients by microprobe step scans. Am. Min., 73: 901-909.

Ganguly, J., Cheng, W., and Chakraborty, S., 1998. Cation diffusion in aluminosilicate garnets: experimental determination in pyrope-almandine diffusion couples. Contrib. Mineral. Petrol., 131: 171-180.

Hermeling, J., and Schmalzried, H., 1984. Tracerdiffusion of the Fe-cations in olivine $(Fe_xMg_{1-x})_2SiO_4$ (III). Phys. Chem. Minerals, 11: 161-166.

Hier-Majumder, S., Anderson, I.M., and Kohlstedt, D.L., 2005. Influence of protons on Fe-Mg interdiffusion in olivine. Jour. Geophys. Res. 110, B02202, doi 10.1029/2004JB003292.

Holzapfel, C., Rubie, D. C., Mackwell, S., and Frost, D. J., 2003. Effect of pressure on Fe-Mg interdiffusion in $(Fe_xMg_{1-x})O$, ferropericlase. Phys. Earth Planet. Int., 139: 21-34.

Holzapfel, C., Rubie, D.C., Frost, D.J., and Langenhorst, F., 2005. Geophysics: Fe-Mg interdiffusion in (Mg,Fe)SiO3 perovskite and lower mantle reequilibration.

Science, 309: 1707-1710.

Ito, M., Yurimoto, H., Morioka, M., and Nagasawa, H., 1999. Co^{2+} and Ni^{2+} diffusion in olivine determined by secondary ion mass spectrometry. Phys. Chem. Min., 26: 425-431.

Jaoul, O., Bertran-Alvarez, Y., Liebermann, R. C., and Price, G. D., 1995. Fe-Mg interdiffusion in olivine up to 9 GPa at T = 600-900°C; experimental data and comparison with defect calculations. Phys. Earth Plan. Int., 89: 199-218.

Jurewicz, A. J. and Watson, E. B., 1988. Diffusion in olivine xenocrysts, with applications to petrology and mineral physics. Contrib. to Min. Petrol., 99: 186-201.

Katsura T., Yamada, H., Osamu Nishikawa, O., Song, M., Kubo, A., Shinmei, T., Yokoshi, S., Aizawa, Y., Yoshino, T., Walter, M. J., Ito, E., 2004. Olivine-wadsleyite transition in the system $(Mg,Fe)_2SiO_4$. J. of Geophysical Research, 109, B02209, doi:10.1029/2003JB002438

Keppler, H., Frost, D.J., 2005. Introduction to minerals under extreme conditions, in: R. Miletich (Editor). Mineral Behaviour at Extreme Conditions, European Mineralogical Union Lecture Notes in Mineralogy, Vol. 7 , EMU, 2005, pp. 1-30.

Kubo, T., Shimojuko, A., and Ohtani, E., 2004. Fe-Mg interdiffusion rates in wadsleyite and the diffusivity jump at the 410 km discontinuity. Phys. Chem. Minerals, 31: 456-464.

Mei, S., and Kohlstedt, D. L., 2000. Influence of water on plastic deformation of olivine aggregates 1. Diffusion creep regime. J. Geophys. Res., 105: 21457-21469.

Meißner, E. and Sharp, T. and Chakraborty, S., 1998. Quantitative measurement of short compositional profiles using analytical transmission electron microscopy. Am. Min., 83: 546-552.

Misener, D. J., 1974. Cationic diffusion in olivine to 1400°C and 35 kbars. In: A. W. Hoffmann, B. J. Giletti, H. S. Yoder, and R. A. Yund (Editors). Geochemical Transports and Kinetics. Carnegie Institution of Washington, 117-129.

Morioka, M., and Nagasawa, H., 1991. Ionic diffusion in olivine. In: J. Ganguly (Editor) Diffusion, Atomic ordering and Mass Transport. Springer, Adv. Phys. Geochem., 8: 176-197.

Nakamura, A., and Schmalzried, H., 1983. On the nonstoichiometry and point defects of olivine. Phys. Chem. Minerals, 10: 27-37.

Nakamura, A. and Schmalzried, H. (1984). On the Fe^{2+}-Mg^{2+} interdiffusion in olivine (II). Ber. Bunsenges. Phys. Chem., 88: 140–145.

Nye, J. F., 1985. Physical Properties of Crystals. Oxford Science Publications, 329 pp.

Paterson, M. S., 1982. The determination of hydroxyl by infrared absorption in quartz,

silicate glasses and similar materials. Bull. Mineral., 105: 20-29.

Petry, C., Chakraborty, S., and Palme, H., 2004. Experimental determination of Ni diffusion coefficients in olivine and their dependence on temperature, composition, oxygen fugacity and crystallographic orientation. Geochimica et Cosmochimica Acta, 68/20: 4179-4188.

Reed, S. J. B., 1996. Electron microprobe analysis and scanning electron microscopy in geology. Cambridge University Press, Cambridge, 201 pp.

Ride, R., 1991. Handbook of Chemistry and Physics. CRC Press, Inc.

Rubie, D. C., 1993. Mechanisms and kinetics of reconstructive phase transformations in the Earth's mantle. In: R. Luth (Editor). Shourt Course handbook on Experiments at High Pressure and Applications to the Earth's Mantle, Mineralogical Association of Canada, Edmonton: 247-303.

Rubie, D. C., Karato, S., Yan, H., and O'Neill, H. S. C., 1993. Low differential stress and controlled chemical environment in multianvil high-pressure experiments. Phys. Chem. Min., 20: 315-322.

Solomatov, V. S., and Stevenson, D. J., 1994. Can sharp seismic discontinuities be caused by non-equilibrium phase transformations? Earth and Plan. Sci. Let., 125: 267-279.

Turcotte, D.L., and Schubert, G., 1982. Geodynamics: Applications of continuum physics to geological problems. John Wiley & Sons, 1982, 450 pp.

Young, D. A., 1991. Phase Diagrams of the Elements. University of California Press.

Figure captions

Figure 1. The central region of the multianvil 14/8 octahedral pressure assembly used for diffusion experiments in this study. The sample consists either of a diffusion couple of two single crystals enclosed in a Au or Ni-NiO capsule. Details of the respective capsules are shown enlarged (centre). W-Re TC denotes $W_{97}Re_3$-$W_{75}Re_{25}$ thermocouple.

Figure 2. Backscattered electron images of run products from the two capsule types used: A gold capsule, B Ni-NiO capsule (see Section 3). The step of the inner $LaCrO_3$ furnace is visible in both A and B.

Figure 3. Examples of concentration profiles in olivine measured by EPMA (electron microprobe). The experiment was performed at 12 GPa, 1623 K and annealed for 72 h (16CS12). In (A) the Fe and the Mg profiles are shown together. The Fe-Mg interdiffusion coefficient can be derived from either of the two profiles. In (B) the Mn profile and in (C) the Ni profile are shown.

Figure 4. Comparison of Fe profiles (concentration normalized to the two end members) measured by EPMA and EDX-STEM for sample 17CS12 (Table 1). For fitting, the data of the analytical solution (Eq. 1), (D_{const}) using the EPMA data and a simulation employing an exponential composition dependence, ($D_{\omega\text{-}dep}$) using the EDX-STEM data were used, as discussed in the text.

Figure 5. Diffusion coefficients as function of pressure for Fe-Mg exchange (A, up-pointing triangles), Ni diffusion (B, down-pointing triangles) and Mn diffusion (C,

circles) at 1673 K. Open symbols represent values at the Ni-NiO buffer, whereas closed symbols are representative of experiments employing Au capsules. In A, for Fe-Mg interdiffusion, linear fits to all data (including the 1 bar value of Chakraborty, 1997) as well as to data from experiments at high pressure employing Ni-NiO capsules only or Au capsules only are shown for comparison. In B, in the case of Ni, the two lines correspond to fits to the Au data only and to all data (including the 1 bar datum from Petry et al., 2004) respectively. In C, for Mn, a linear fit utilizing all data as well as the fit for Fe-Mg interdiffusion using all data are shown. For all components, the data point at 11 GPa was excluded as discussed in the text.

Figure 6. Diffusion coefficients as a function of inverse temperature for Fe-Mg exchange (A), Ni diffusion (B) and Mn diffusion (C) at 12 GPa. Symbols are the same as used in Figure 5. For all components, experiments using Au capsules are shown. In addition, a single datum (open symbol) from an experiment using a Ni capsule is also shown in all three cases. The fit lines correspond to linear fits for determining the activation energy as described in the text.

Figure 7. Comparison of results for Fe-Mg interdiffusion, Ni diffusion and Mn diffusion as function of inverse temperature.

Figure 8. Comparison of the results obtained in this study for Fe-Mg interdiffusion with results of other high pressure studies in the literature. All values are normalized to $X_{Fe_2SiO_4} = 0.03$ at 1673 K at an fO_2 corresponding to the Ni-NiO buffer. Note the discussion regarding the datum at 11 GPa from the study of Chakraborty et al. (1999) in the text.

Figure 9. Calculated diffusion coefficients as function of depth in the mantle. One calculation neglects the pressure effect whereas the other calculation employs a value of 5.3 cm^3/mole for the activation volume. The inset shows the estimated temperature variation in the mantle along a lithospheric geotherm (Turcotte and Schubert, 1982) and a typical mantle adiabat (Katsura et al., 2004) on which the calculated diffusion coefficients are based.

Table 1. Results and conditions of the olivine high pressure diffusion runs - Diffusion coefficients are given in logarithm of [D in m^2/sec].

Sample	Capsule	T, K	**P**, GPa	t, min	**log (D_{Fe-Mg})**	**log (D_{Ni})**	**log (D_{Mn})]**
1CS12	Au	1673	12	1440	-16.2(3)	-16.5(4)	-16.1(5)
2CS10	Au	1673	10	1440	-16.4(3)	-15.5(4)	-16.4(5)
3CS8	Au	1673	8	1440	-15.6(3)	-15.7(4)	-15.8(5)
4CS11	Au	1673	11	1440	-15.5(3)	-15.7(4)	-15.4(5)
5CS12	Au	1673	12	1440	-16.3(3)	-16.4(4)	-16.1(5)
6CS10	Au	1673	10	1440	-16.3(3)	-15.5(4)	-16.5(5)
7CS11.5	Au	1673	11.5	1440	-16.1(3)	-15.8(4)	-16.2(5)
8CS10.5	Au	1673	10.5	1440	-16.1(3)	-15.5(4)	-15.9(5)
9CS11	Au	1673	11	1440	-15.3(3)	-15.4(4)	-15.5(5)
10CS11.5	Au	1673	11.5	1440	-16.3(3)	-16.1(4)	-16.3(5)
13CS12	Au	1773	12	1440	-15.9(3)	-16.1(4)	-16.0(5)
14CS12	Au	1723	12	1440	-16.1(3)	-16.3(4)	-16.2(5)
15CS12	Au	1823	12	1440	-15.5(3)	-15.6(4)	-15.6(5)
16CS12	Au	1623	12	4320	-16.8(3)	-16.9(4)	-16.5(5)
17CS12	Ni-NiO	1673	12	1443	-16.7(3)	-16.6(4)	-16.7(5)
18CS6	Ni-NiO	1673	6	1440	-15.7(3)	n.d.[1]	n.d[1].
20CS6	Ni-NiO	1673	6	1440	-15.4(3)	-15.4(3)	-15.5(5)

[1]Ni and Mn diffusion coefficients were not determined in Run # 18CS6 due to slight Mn contamination of the sample from the capsule material.

Table 2. ***Activation volumes for Fe-Mg interdiffusion, Ni diffusion, and Mn diffusion in olivine in units of cm^3/mol. The left column indicates the data and experiments that were included in the various fits.***

Exp	V_a(Fe-Mg)	V_a(Ni)	V_a(Mn)
Ni-NiO (excl. 1 bar)	6.1(1.4)	6.4(n.d.)	6.4(n.d)
Ni-NiO (incl. 1 bar)	6.3(0.6)	7.0(0.4)	-
Au (excl. 1 bar)	3.8(1.8)	6.6(2.9)	0.07(2.9)
Au (incl. 1 bar)	5.3(0.6)	5.8(0.9)	
All (excl. 1 bar)	4.6(0.9)	5.4(1.8)	4.6(1.7)
All (incl. 1 bar)	5.3(0.6)	5.8(0.9)	-

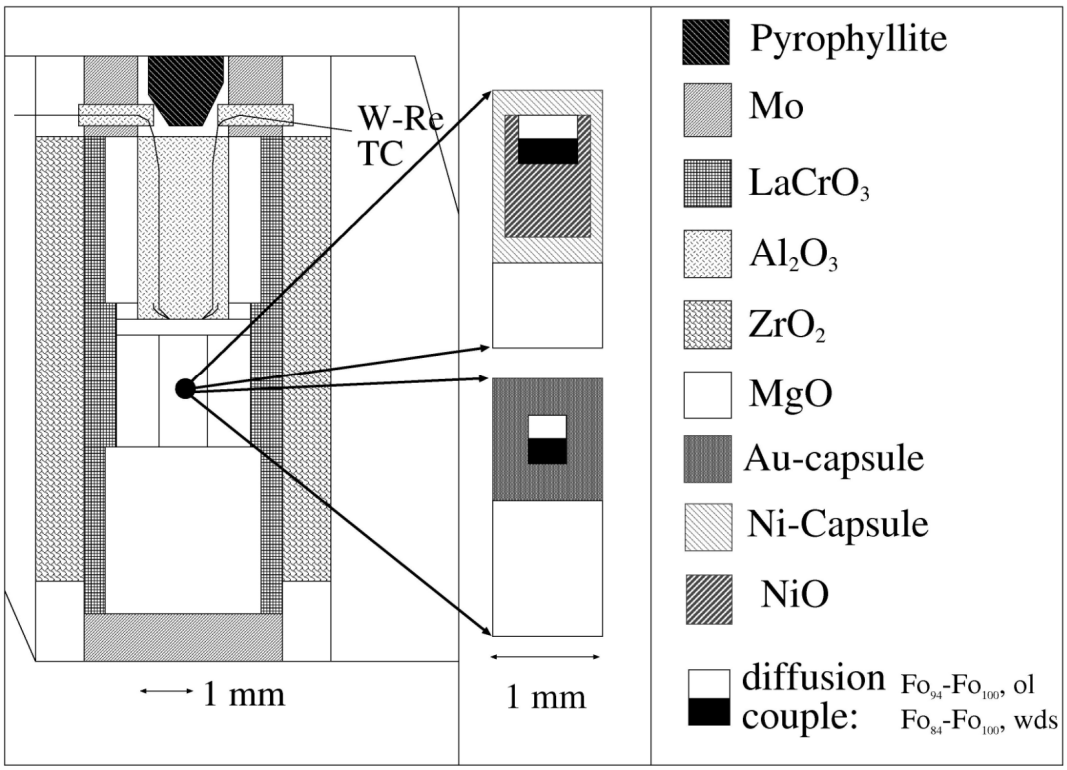

Fig. 1

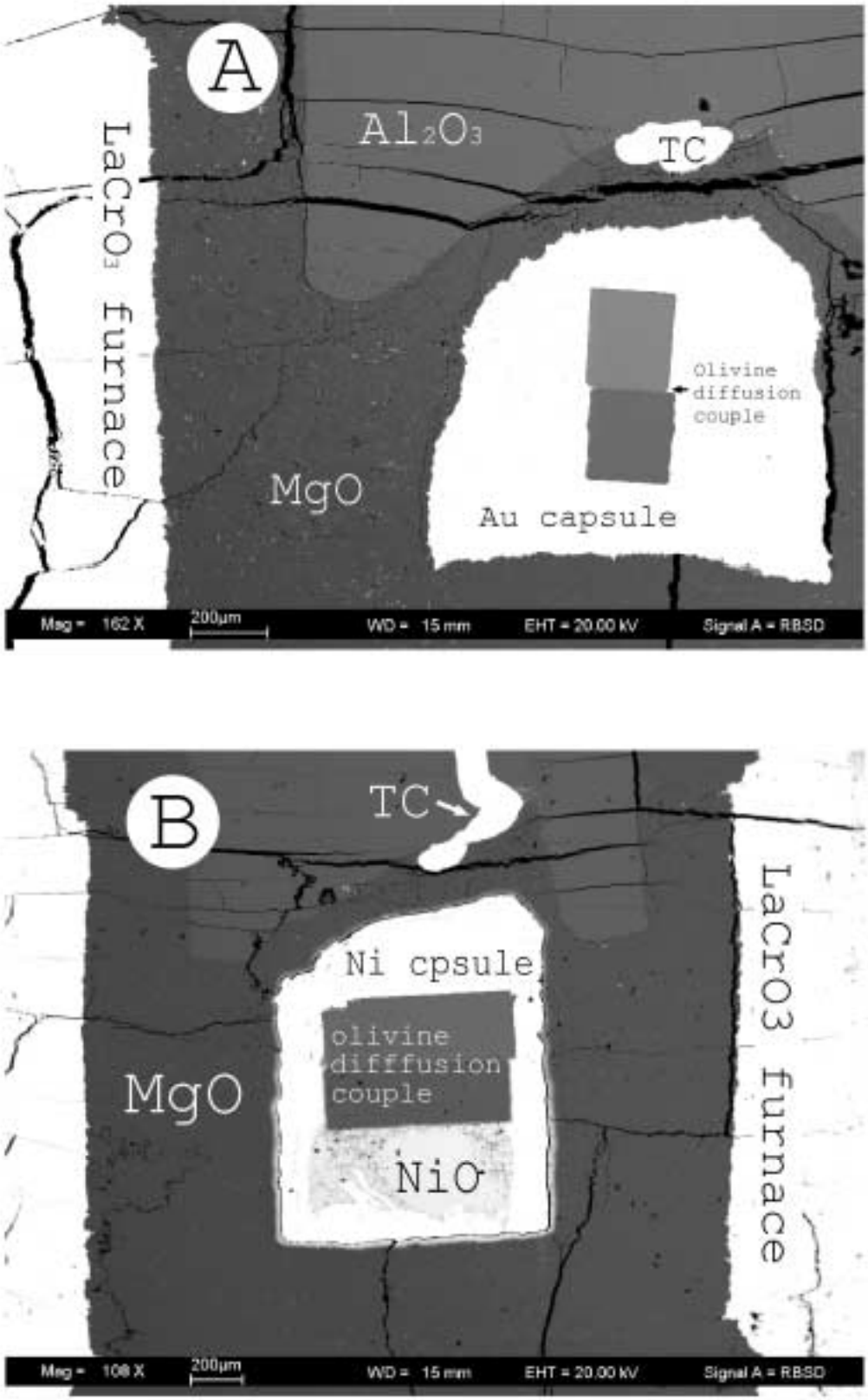

Fig 2.

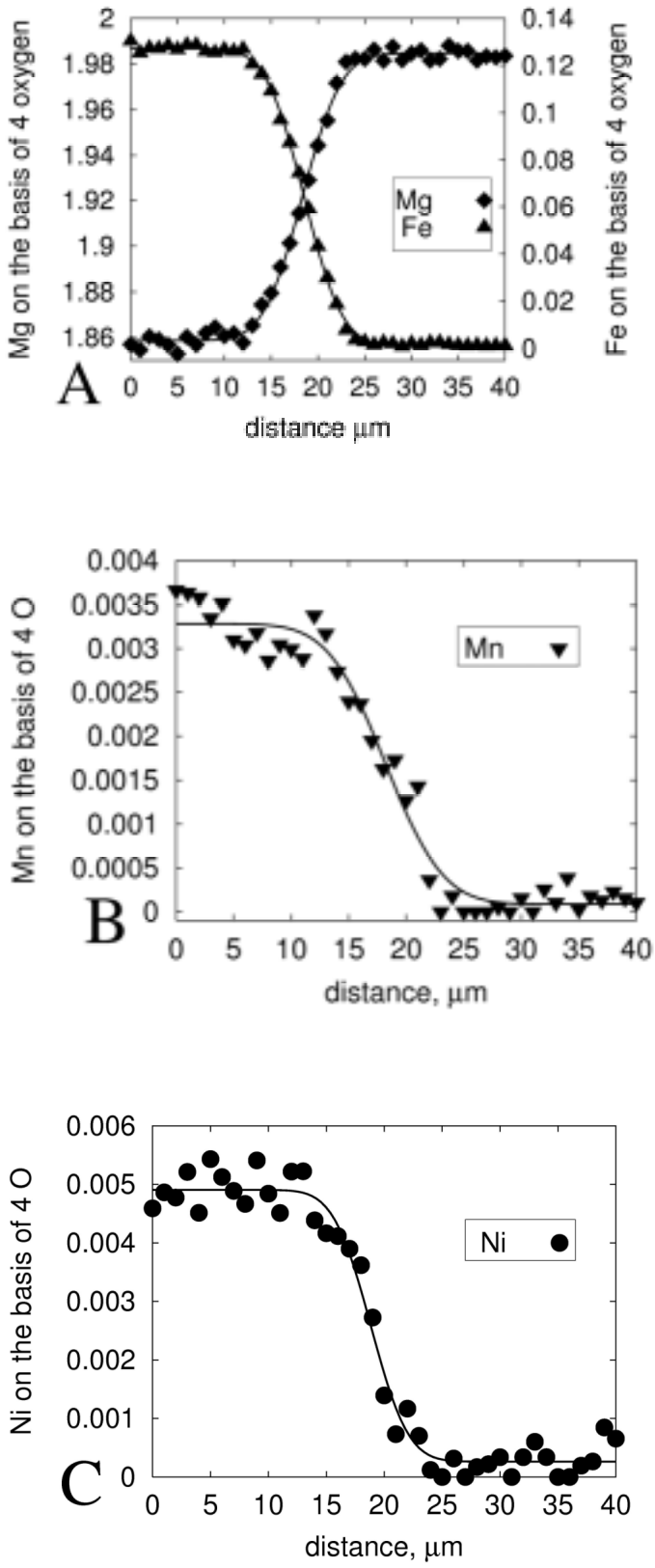

Fig. 3

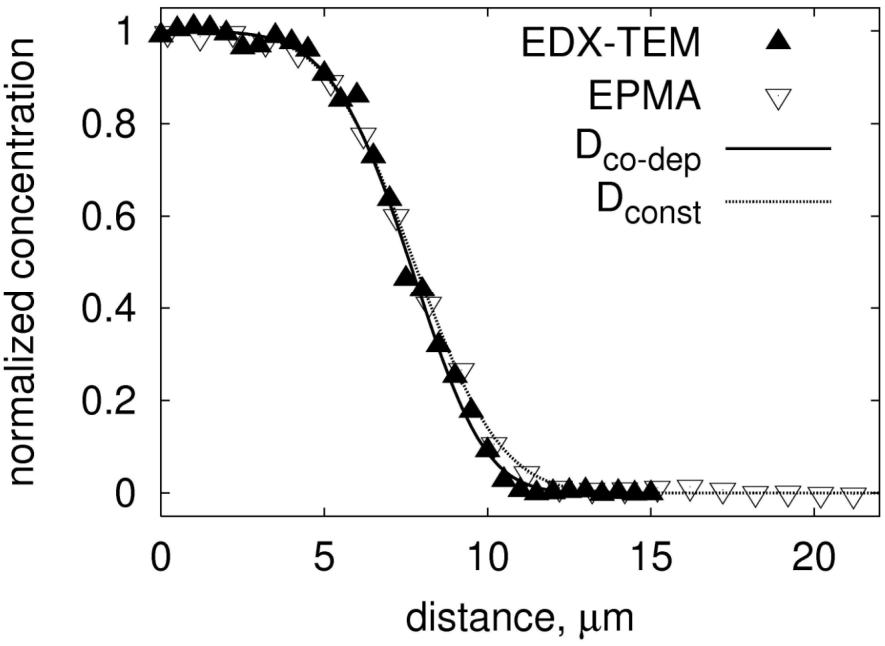

Figure 4

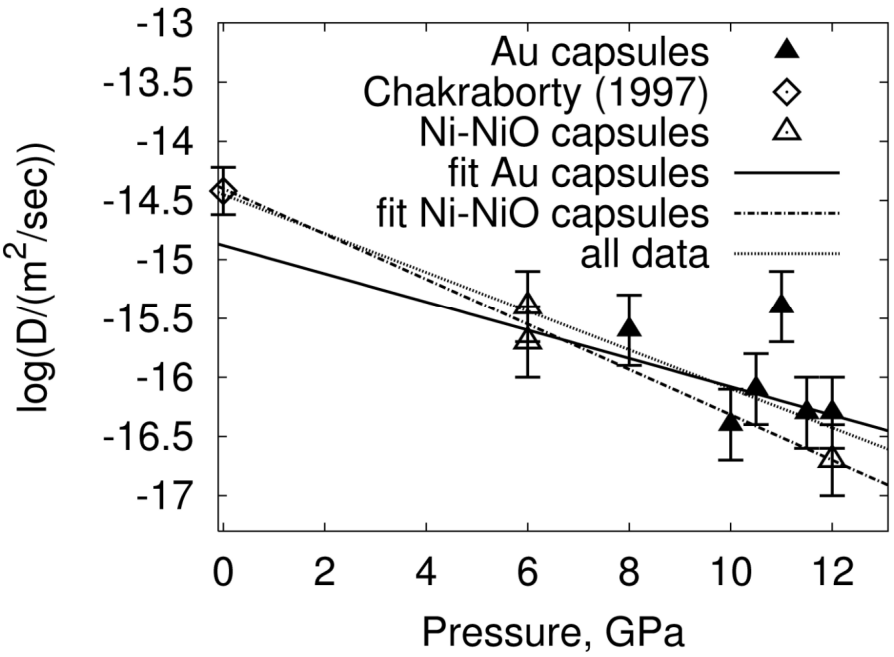

Figure 5A

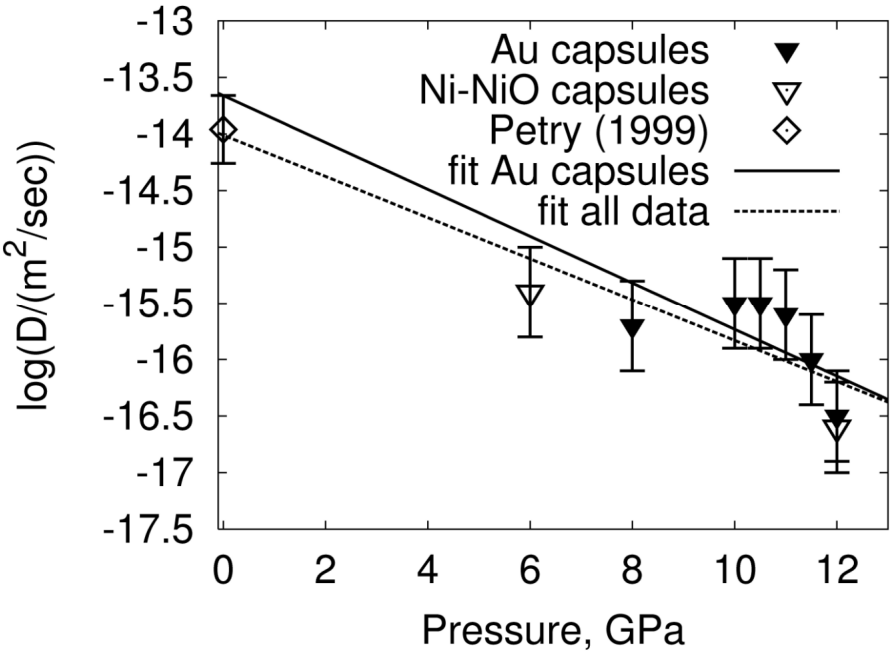

Figure 5B

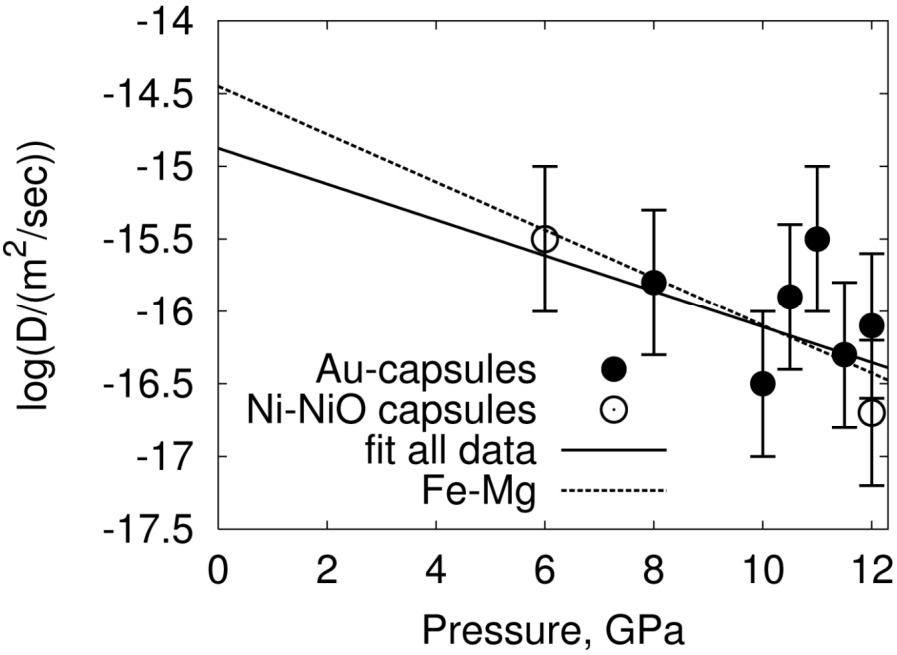

Figure 5C

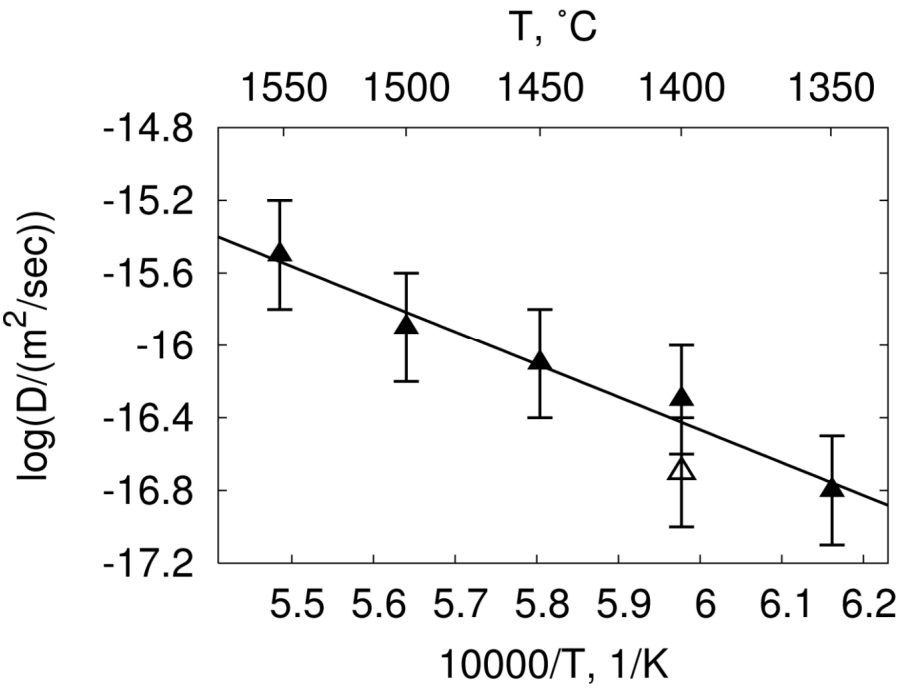

Figure 6A

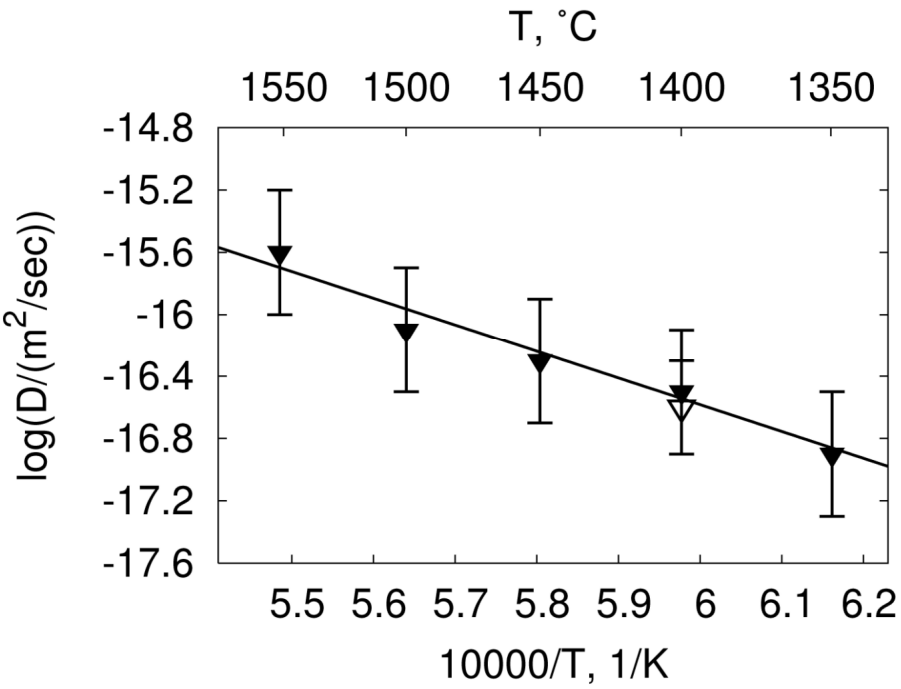

Figure 6B

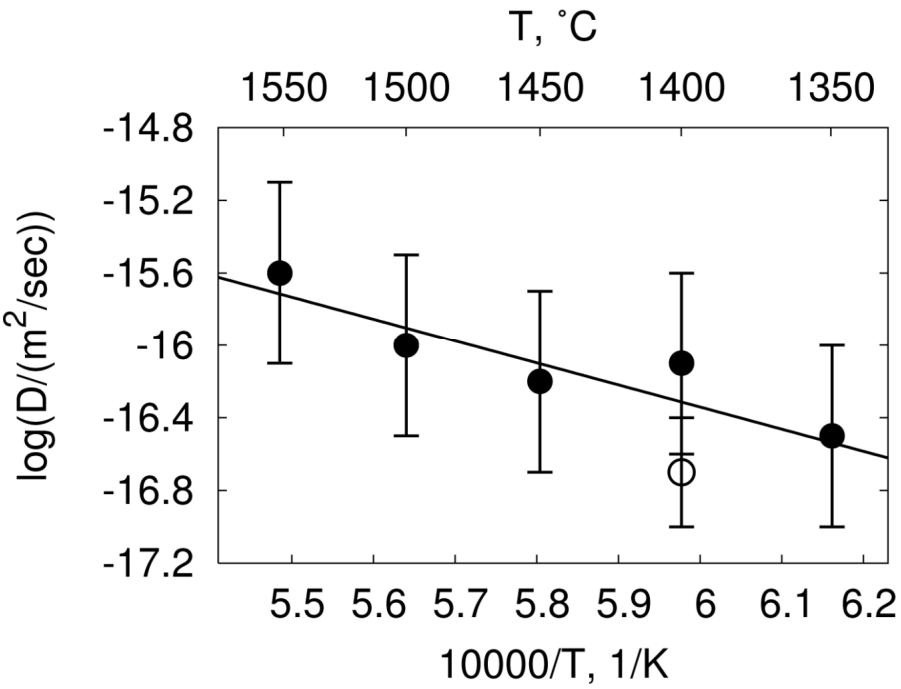

Figure 6C

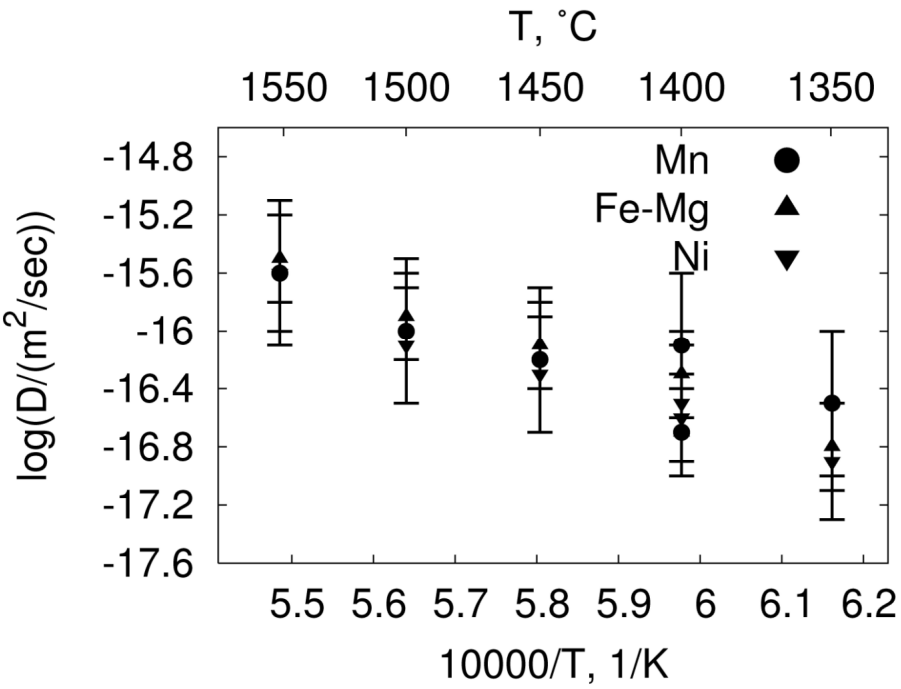

Figure 7

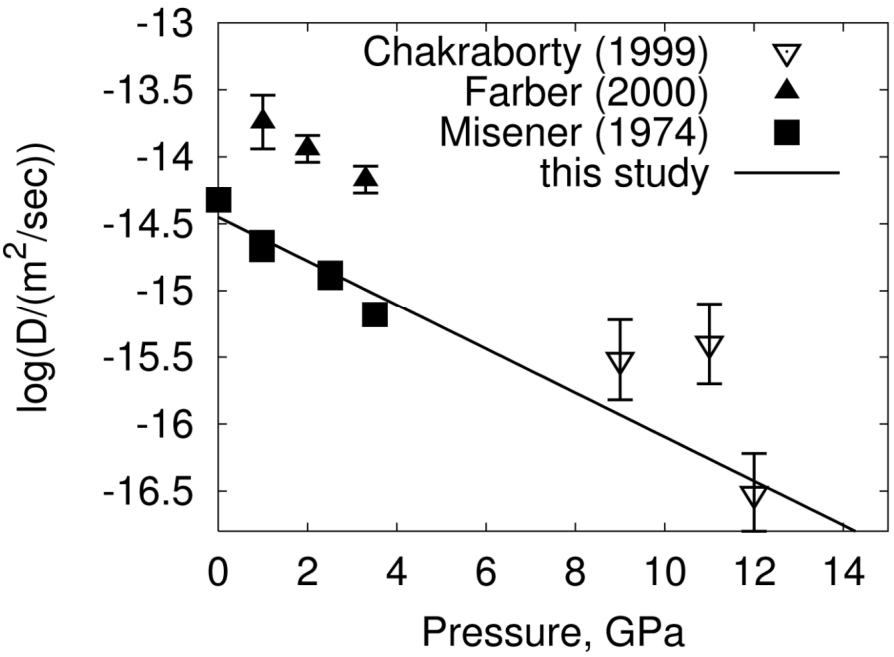

Figure 8

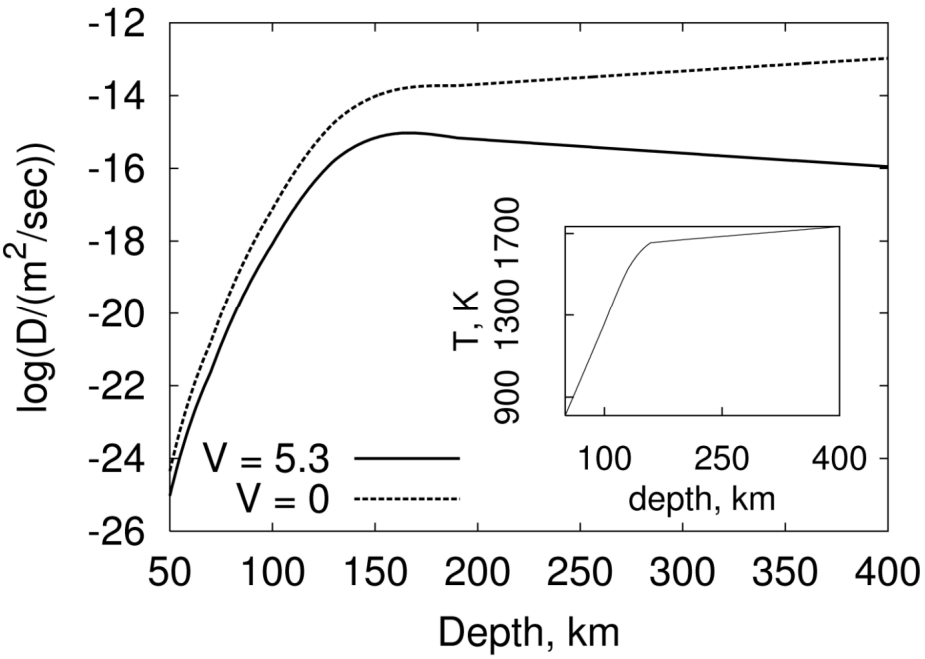

Figure 9